Simulation of molecular ring emission spectra - LH4 complex: localization of exciton states and dynamics

Milan Horák, Pavel Heřman, David Zapletal

***Abstract*—**Absorption and steady state fluorescence spectra and localization of exciton states for ring molecular systems are presented. The cyclic antenna units LH2 and LH4 of the bacterial photosystem from purple bacterium *Rhodopseudomonas acidophila* and *Rhodopseudomonas palustris* can be modeled by such systems. The cumulant-expansion method of Mukamel et al. is used for the calculation of spectral responses of the system. Dynamic disorder, interaction with a bath, in Markovian approximation simultaneously with uncorrelated static disorder in local excitation energies are taking into account in our simulations. We also discuss different types of exciton dynamics, that are coupled to above mentioned effects and compare the results in that the dynamic disorder is taken into account with the results without dynamic disorder.

***Keywords*—**LH2, LH4, fluorescence spectrum, absorption spectrum, static and dynamic disorder, exciton states, localization, *Mathematica*

I. Introduction

Photosynthesis starts with the absorption of a solar photon by one of the light-harvesting pigment-protein complexes and transferring the excitation energy to the photosynthetic reaction center, where a charge separation is initiated. These initial ultrafast events have been extensively investigated. Knowledge of the microscopic structure of some photosynthetic systems, e.g., photosynthetic systems of purple bacteria, invokes during last twenty years long and intensive effort of many theoretical and experimental laboratories. No final conclusion about the character of exited states, energy transfer, etc. can be generally drawn.

The antenna systems of photosynthetic units from purple bacteria are formed by ring units LH1, LH2, LH3, and LH4. The geometric structure is known in great detail from X-ray crystallography, e.g., for the LH2 complex of the purple bacterium *Rhodopseudomonas acidophila* [1], [2]. The bacteriochlorophyll (BChl) molecules are organized in two concentric rings. One ring features a group of nine well-separated BChl molecules (B800) with absorption band at about 800 nm. The other ring consists of eighteen closely packed BChl molecules (B850) absorbing around 850 nm. LH2 complexes from other purple bacteria have analogous ring structures. The similar ring structure but with larger number of BChl molecules is supposed for LH1 rings. The intermolecular distances under 1 nm in rings determine strong exciton couplings between corresponding pigments. Complexes LH3 and LH4 with modified structure (*Rhodopseudomonas palustris*) have been also discovered [3]. While the B850 dipole moments in LH2 ring have tangential arrangements, in the LH4 one they are oriented more radially. Mutual interaction of the nearest neighbour BChls is therefore two times smaller and has opposite sign. Besides ring with sixteen BChl molecules, an additional BChl ring is also present in LH4 complex.

Due to the strong interaction between BChl molecules, an extended Frenkel exciton states model is considered in our theoretical approach. In spite of extensive investigation, the role of the protein moiety in governing the dynamics of the excited states has not been totally clear yet. At room temperature the solvent and protein environment fluctuate with characteristic time scales ranging from femtoseconds to nanoseconds. The simplest approach is to substitute fast fluctuations by dynamic disorder and slow fluctuations by static disorder.

Static disorder effect on the anisotropy of fluorescence for LH2 rings was studied by Kumble and Hochstrasser [4] and Nagarajan et al. [5]–[7]. We extended these investigations by consideration of dynamic disorder. We studied this effect for simple model systems [8]–[10] and then for the models of LH2 rings [11], [12]. Various types of the uncorrelated static disorder (in local excitation energies, in transfer integrals, etc.) and correlated one (e.g., elliptical deformation) were used in the past [12]–[15] and also different arrangements of optical dipole moments were compared [16]–[19].

Recently we have focused on the modeling of the steady state fluorescence and absorption spectra for LH2 complex [20], [21]. In addition, we have investigated the exciton state localization of this complex and also time dependence of exciton density matrix [22], [23]. Main goal of this paper is the presentation of the steady state fluorescence and absorption spectra simulations for LH4 ring. In our simulations the dynamic disorder (interaction with the phonon bath) in

Manuscript received October 2, 2012.

This work was supported in part by the Faculty of Education, University of Hradec Králové (project of specific research No. 2131/2012 - M. Horák and P. Heřman).

M. Horák is with the Faculty of Education, University of Hradec Králové, Rokitanského 62, 50003 Hradec Králové, Czech Republic (e-mail: milan.horak@uhk.cz).

P. Heřman is with the Department of Physics, Faculty of Science, University of Hradec Králové, Rokitanského 62, 50003 Hradec Králové, Czech Republic (e-mail: pavel.herman@uhk.cz).

D. Zapletal is with the Institute of Mathematics, Faculty of Economics and Administration, University of Pardubice, Studentská 95, 53210 Pardubice, Czech Republic (e-mail: david.zapletal@upce.cz).

Markovian approximation is taken into account simultaneously with uncorrelated static disorder in local excitation energies. In addition, we present the comparison of the results relating to the exciton state localization for LH2 complex with our new results for LH4 one.

Present paper is the extension of our contribution [24] presented on WSEAS conference MACMESE'12. The rest of the paper is structured as follows. Section II. introduces the ring model with the uncorrelated static disorder and dynamic disorder (interaction with phonon bath) and the cumulant expansion method of Mukamel et al. [25], [26], which is used for the calculation of spectral responses of the system with exciton-phonon coupling, is presented . Also the quantities describing localization of exciton states and the equations for time development of exciton density matrix are shown here. In Section III. the computational point of view for our calculations is discussed. The presented results of our simulations and used units and parameters could be found in Section IV. In Section V. some conclusions are drawn.

II. Physical model

We assume that only one excitation is present on the ring after an impulsive excitation. The Hamiltonian of an exciton in the ideal ring coupled to a bath of harmonic oscillators reads

$$H = H_{\rm ex}^0 + H_{\rm ph} + H_{\rm ex-ph} + H_{\rm s}. \tag{1}$$

Here the first term,

$$H_{\rm ex}^0 = \sum_{m,n(m\neq n)} J_{mn} a_m^\dagger a_n, \tag{2}$$

corresponds to an exciton, e.g. the system without any disorder. The operator $a_m^\dagger$ (a_m) creates (annihilates) an exciton at site m, J_{mn} (for $m \neq n$) is the so-called transfer integral between sites m and n. The second term,

$$H_{\rm ph} = \sum_q \hbar\omega_q b_q^\dagger b_q, \tag{3}$$

represents phonon bath in the harmonic approximation (the phonon creation and annihilation operators are denoted by $b_q^\dagger$ and b_{-q}, respectively). The third term in (1),

$$H_{\rm ex-ph} = \frac{1}{\sqrt{N}} \sum_m \sum_q G_q^m \hbar\omega_q a_m^\dagger a_m (b_q^\dagger + b_{-q}), \tag{4}$$

describes exciton-phonon interaction which is assumed to be site-diagonal and linear in the bath coordinates (the term G_q^m denotes the exciton-phonon coupling constant). The last term in (1), $H_{\rm s}$, corresponds to static disorder. Influence of uncorrelated static disorder is modeled by the local excitation energy fluctuations $\delta\varepsilon_n$ with Gaussian distribution and standard deviation Δ

$$H_{\rm s} = \sum_n \delta\varepsilon_n a_n^\dagger a_n. \tag{5}$$

Inside one ring the pure exciton Hamiltonian can be diagonalized using the wave vector representation with corresponding delocalized "Bloch" states α and energies E_α. Considering homogeneous case with only nearest neighbour transfer matrix elements

$$J_{mn} = J_0(\delta_{m,n+1} + \delta_{m,n-1}) \tag{6}$$

and using Fourier transformed excitonic operators (Bloch representation)

$$a_\alpha = \sum_n {\rm e}^{{\rm i}\alpha kn},\ \alpha = \frac{2\pi}{N} l,\ l = 0, \pm 1, \ldots, \pm\frac{N}{2}, \tag{7}$$

the simplest exciton Hamiltonian in α - representation reads

$$H_{\rm ex}^0 = \sum_\alpha E_\alpha a_\alpha^\dagger a_\alpha, \quad E_\alpha = -2J_0 \cos\alpha. \tag{8}$$

The cumulant-expansion method of Mukamel et al. [25], [26] is used for the calculation of spectral responses of the system with exciton-phonon coupling. Absorption $OD(\omega)$ and steady-state fluorescence $FL(\omega)$ spectrum can be expressed as

$$OD(\omega) = \omega \sum_\alpha d_\alpha^2 \times \\ \times {\rm Re} \int_0^\infty dt {\rm e}^{{\rm i}(\omega-\omega_\alpha)t - g_{\alpha\alpha\alpha\alpha}(t) - R_{\alpha\alpha\alpha\alpha}t}, \tag{9}$$

$$FL(\omega) = \omega \sum_\alpha P_\alpha d_\alpha^2 \times \\ \times {\rm Re} \int_0^\infty dt {\rm e}^{{\rm i}(\omega-\omega_\alpha)t + {\rm i}\lambda_{\alpha\alpha\alpha\alpha}t - g^*_{\alpha\alpha\alpha\alpha}(t) - R_{\alpha\alpha\alpha\alpha}t}. \tag{10}$$

Here $\vec{d}_\alpha = \sum_n c_n^\alpha \vec{d}_n$ is the dipole strength of eigenstate α, c_n^α are the expansion coefficients of the eigenstate α in site representation and P_α is steady state population of the eigenstate α. The inverse lifetime of exciton state $R_{\alpha\alpha\alpha\alpha}$ [27] is given by the elements of Redfield tensor $R_{\alpha\beta\gamma\delta}$ [28]. It is a sum of the relaxation rates between exciton states, $R_{\alpha\alpha\alpha\alpha} = -\sum_{\beta\neq\alpha} R_{\beta\beta\alpha\alpha}$. The g-function and λ-values in (10) are given by

$$g_{\alpha\beta\gamma\delta} = -\int_{-\infty}^{\infty} \frac{d\omega}{2\pi\omega^2} C_{\alpha\beta\gamma\delta}(\omega) \times \\ \times \left[\coth\frac{\omega}{2k_{\rm B}T} (\cos\omega t - 1) - {\rm i}(\sin\omega t - \omega t) \right], \tag{11}$$

$$\lambda_{\alpha\beta\gamma\delta} = -\lim_{t\to\infty} \frac{d}{dt} {\rm Im}\{g_{\alpha\beta\gamma\delta}(t)\} = \\ = \int_{-\infty}^{\infty} \frac{d\omega}{2\pi\omega} C_{\alpha\beta\gamma\delta}(\omega). \tag{12}$$

The matrix of the spectral densities $C_{\alpha\beta\gamma\delta}(\omega)$ in the eigenstate (exciton) representation reflects one-exciton states coupling to the manifold of nuclear modes. In what follows only a diagonal exciton phonon interaction in site representation is used (see (1)), i.e., only fluctuations of the pigment site energies are assumed and the restriction to the completely uncorrelated dynamical disorder is applied. In such case each site (i.e. each chromophore) has its own bath completely uncoupled from the

baths of the other sites. Furthermore it is assumed that these baths have identical properties [13], [29], [30]

$$C_{mnm'n'}(\omega) = \delta_{mn}\delta_{mm'}\delta_{nn'}C(\omega). \tag{13}$$

After transformation to exciton representation we have

$$C_{\alpha\beta\gamma\delta}(\omega) = \sum_n c_n^\alpha c_n^\beta c_n^\gamma c_n^\delta C(\omega). \tag{14}$$

Various models of spectral density of the bath are used in literature [27], [31], [32]. In our present investigation we have used the model of Kühn and May [31]

$$C(\omega) = \Theta(\omega) j_0 \frac{\omega^2}{2\omega_c^3} \mathrm{e}^{-\omega/\omega_c} \tag{15}$$

which has its maximum at $2\omega_c$.

Delocalization of the exciton states contributing to the steady state FL spectrum can be characterized by the thermally averaged participation ratio $\langle PR \rangle$, which is given by

$$\langle PR \rangle = \frac{\sum_\alpha PR_\alpha \ \mathrm{e}^{-\frac{E_\alpha}{k_B T}}}{\sum_\alpha \mathrm{e}^{-\frac{E_\alpha}{k_B T}}}, \tag{16}$$

where

$$PR_\alpha = \sum_{n=1}^{N} |c_n^\alpha|^4. \tag{17}$$

Time evolution of exciton density matrix $\rho_{\alpha\beta}$ is governed by Redfield equation [28],

$$\frac{\partial \rho_{\alpha\beta}(t)}{\partial t} = -\mathrm{i}\omega_{\alpha\beta}\rho_{\alpha\beta}(t) + \sum_{\gamma\delta} R_{\alpha\beta\gamma\delta}\rho_{\gamma\delta}(t), \tag{18}$$

which is equivalent to Čápek's equation [13]. Exciton density matrix in site representation is given by

$$\rho_{mn} = \sum_{\alpha\beta} c_n^\alpha c_n^\beta \rho_{\alpha\beta}. \tag{19}$$

III. Computational Point of View

To have steady state fluorescence spectrum $FL(\omega)$ and absorption spectrum $OD(\omega)$, it is necessary to calculate single ring $FL(\omega)$ spectrum and $OD(\omega)$ spectrum for large number of different static disorder realizations created by random number generator. Finally these results have to be averaged over all realizations of static disorder. Time evolution of exciton density matrix has to be calculate also for each realization of static disorder. That is why it was necessary to put through numerical integrations for each realization of static disorder (see (10)).

For the most of our calculations the software package *Mathematica* [33] was used. This package is very convenient and has very wide range of applications in different areas of research [34]–[36] not only for symbolic calculations [37] which are needed for expression of all required quantities, but it can be used also for numerical ones [38]. That is why the software package *Mathematica* was used by us as for symbolic calculations as for numerical integrations and also for final averaging of results over all realizations of static disorder.

As concerns the time development of our system, for the solution of the Redfield equation we have used the program written in Fortran and standard Runge-Kutta method.

IV. Results

Above mentioned uncorrelated static disorder in local excitation energies has been taken into account in our simulations simultaneously with dynamic disorder in Markovian approximation. Dimensionless energies normalized to the transfer integral $J_{12} = J_0$ in LH2 ring and dimensionless time τ have been used. Estimation of J_0 varies in literature between 250 cm^{-1} and 400 cm^{-1}. For these extreme values of J_0 our time unit ($\tau = 1$) corresponds to 21.2 fs or 13.3 fs.

The values of transfer integrals in LH4 ring differ from that of LH2 ring. Furthermore, stronger dimerization can be found in LH4 in comparison with LH2 [3]. Therefore we have taken the values of transfer integrals in LH4 ring as follows: $J_{12}^{LH4} = -0.5 J_{12}^{LH2} = -0.5 J_0$,

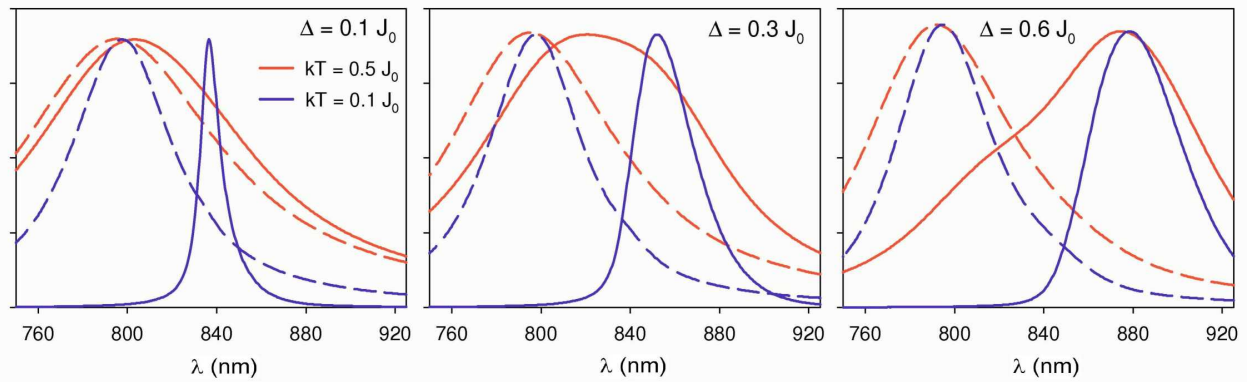

Fig. 1. Resulting absorption $OD(\omega)$ (dashed lines) and steady-state fluorescence $FL(\omega)$ spectra (solid lines) of LH4 ring at room temperature $kT = 0.5\ J_0$ (red lines) and low one $kT = 0.1\ J_0$ (blue lines) averaged over 2000 realizations of Gaussian uncorrelated static disorder in local excitation energies $\delta\varepsilon$ – three strengths $\Delta = 0.1,\ 0.3,\ 0.6\ J_0$.

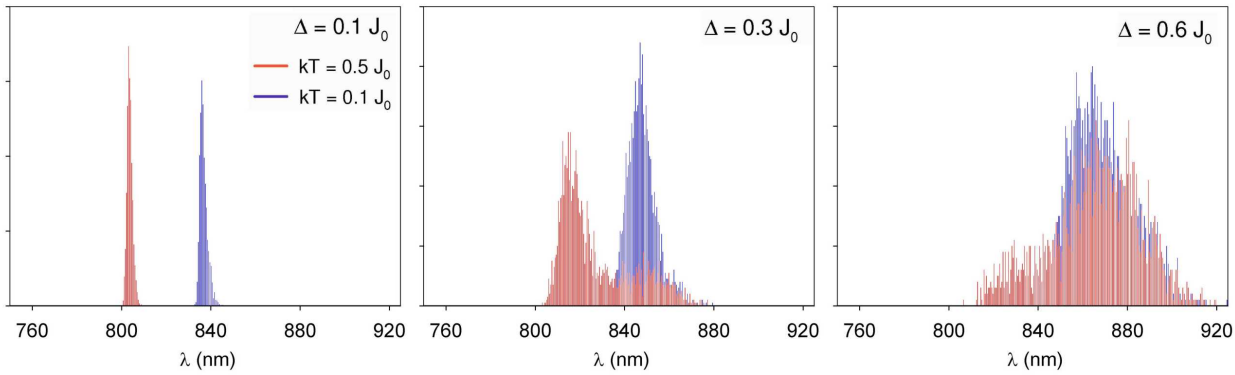

Fig. 2. Peak position distributions of calculated steady-state single ring fluorescence spectra $FL(\omega)$ of LH4 ring at room temperature $kT = 0.5\ J_0$ (red lines) and low one $kT = 0.1\ J_0$ (blue lines) for 2000 realizations of Gaussian uncorrelated static disorder in local excitation energies $\delta\varepsilon$ – three strengths $\Delta = 0.1,\ 0.3,\ 0.6\ J_0$.

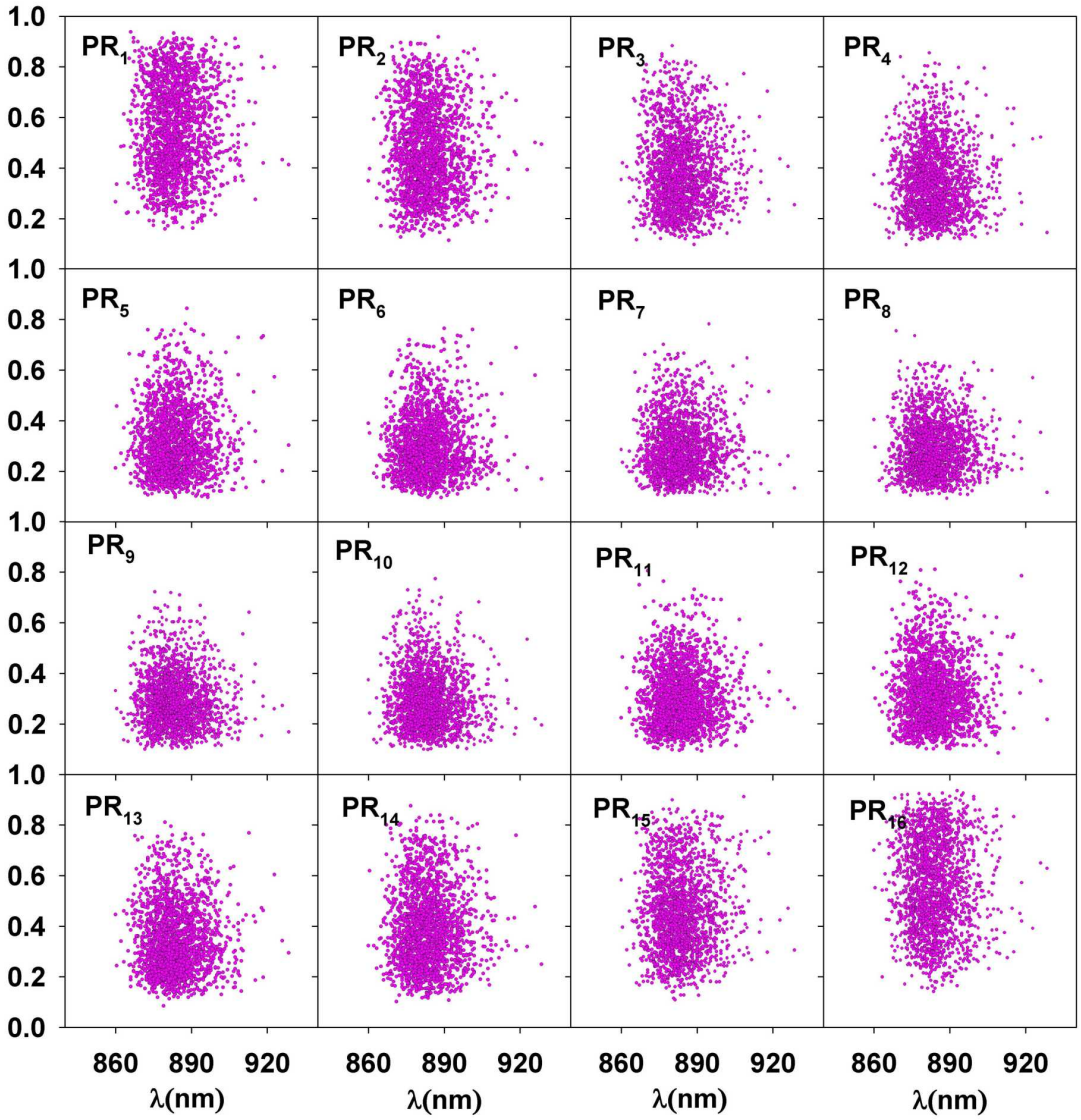

Fig. 3. The distributions of PR_α values ($\alpha = 1, \ldots, 16$) of LH4 ring as a function of FL spectrum peak position at room temperature $kT = 0.5\ J_0$ calculated for 2000 realizations of Gaussian uncorrelated static disorder in local excitation energies $\delta\varepsilon$, for the highest strength $\Delta = 0.6\ J_0$.

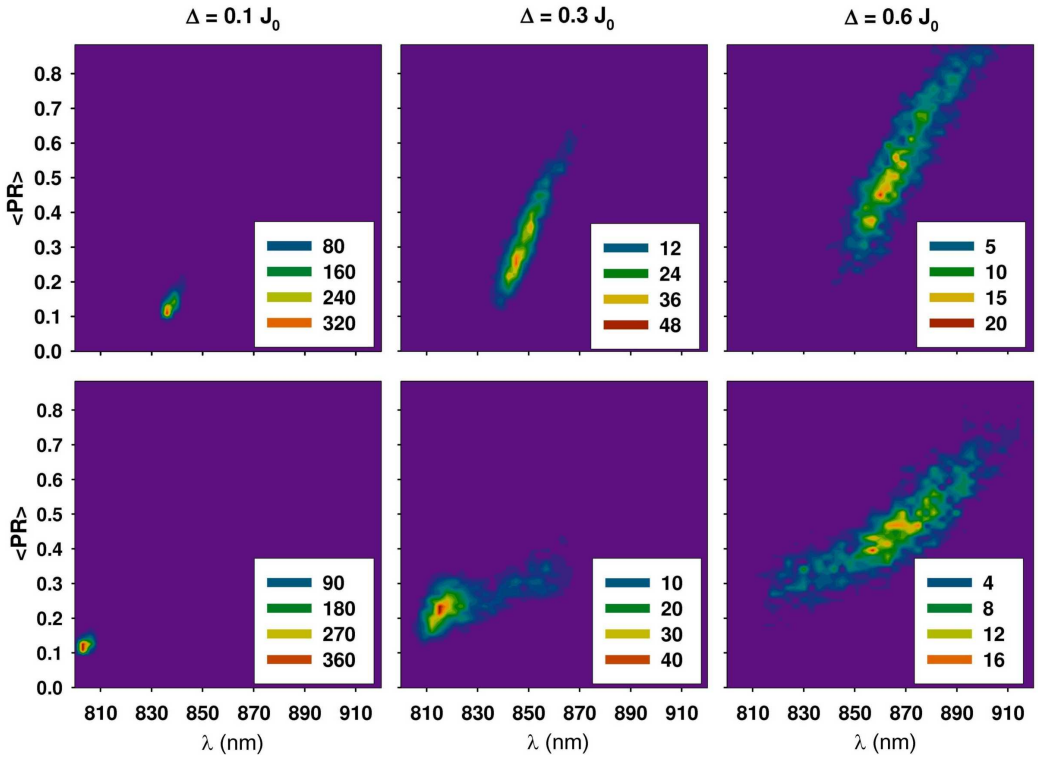

Fig. 4. The distribution of $\langle PR \rangle$ values of LH4 ring as a function of FL spectrum peak position at low temperature $kT = 0.1\ J_0$ (first row) and room temperature $kT = 0.5\ J_0$ (second row), calculated for 2000 realizations of Gaussian uncorrelated static disorder in local excitation energies $\delta\varepsilon_n$ – three strengths Δ = 0.1, 0.3, 0.6 J_0.

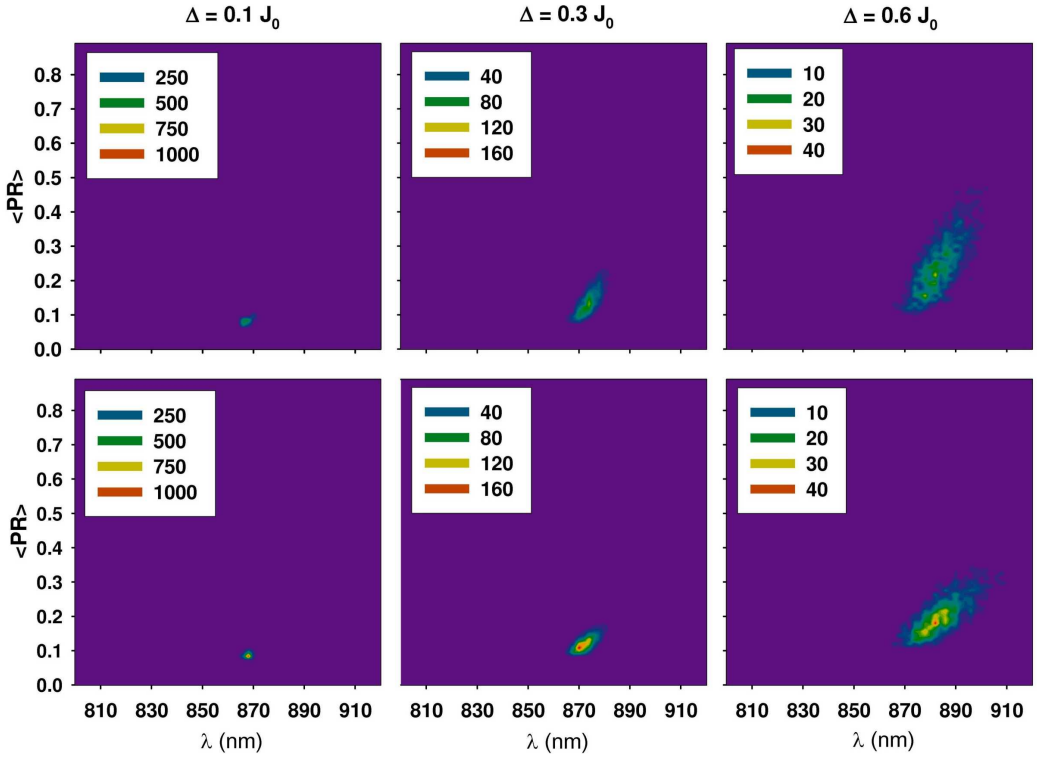

Fig. 5. The distribution of $\langle PR \rangle$ values of LH2 ring as a function of FL spectrum peak position at low temperature $kT = 0.1\ J_0$ (first row) and room temperature $kT = 0.5\ J_0$ (second row), calculated for 2000 realizations of Gaussian uncorrelated static disorder in local excitation energies $\delta\varepsilon_n$ – three strengths Δ = 0.1, 0.3, 0.6 J_0.

$J_{23}^{LH4} = 0.5 J_{12}^{LH4} = -0.25 J_0$. All our simulations of LH4 spectra have been done with the same values of J_0 and unperturbed transition energy from the ground state ΔE_0, that we found for LH2 ring [21].

Contrary to Novoderezhkin et al. [27], different model of spectral density (the model of Kühn and May [12]) has been used. In agreement with our previous results [16], [19] we have used the strength of dynamic disorder $j_0 = 0.4\ J_0$ and cut-off frequency $\omega_c = 0.212\ J_0$ (see (15)). The strengths of uncorrelated static disorder has been taken in agreement with [39]: $\Delta = 0.1,\ 0.3,\ 0.6\, J_0$,.

Resulting absorption $OD(\omega)$ and steady state fluorescence spectra $FL(\omega)$ for LH4 ring at room temperature ($kT = 0.5\ J_0$) and low one ($kT = 0.1\ J_0$) averaged over 2000 realizations of static disorder for three strengths Δ can be seen in Fig. 1.

Fig. 2 presents the peak positions distributions of calculated steady state single ring fluorescence spectra at room temperature $kT = 0.5\ J_0$ and low one $kT = 0.1\ J_0$ for 2000 realizations of static disorder. The distributions are shown for three strengths of static disorder mentioned above.

The distributions of the participation ratios PR_α for each of sixteen eigenstates α can be seen in Fig. 3 for highest strength of static disorder ($\Delta = 0.6\, J_0$).

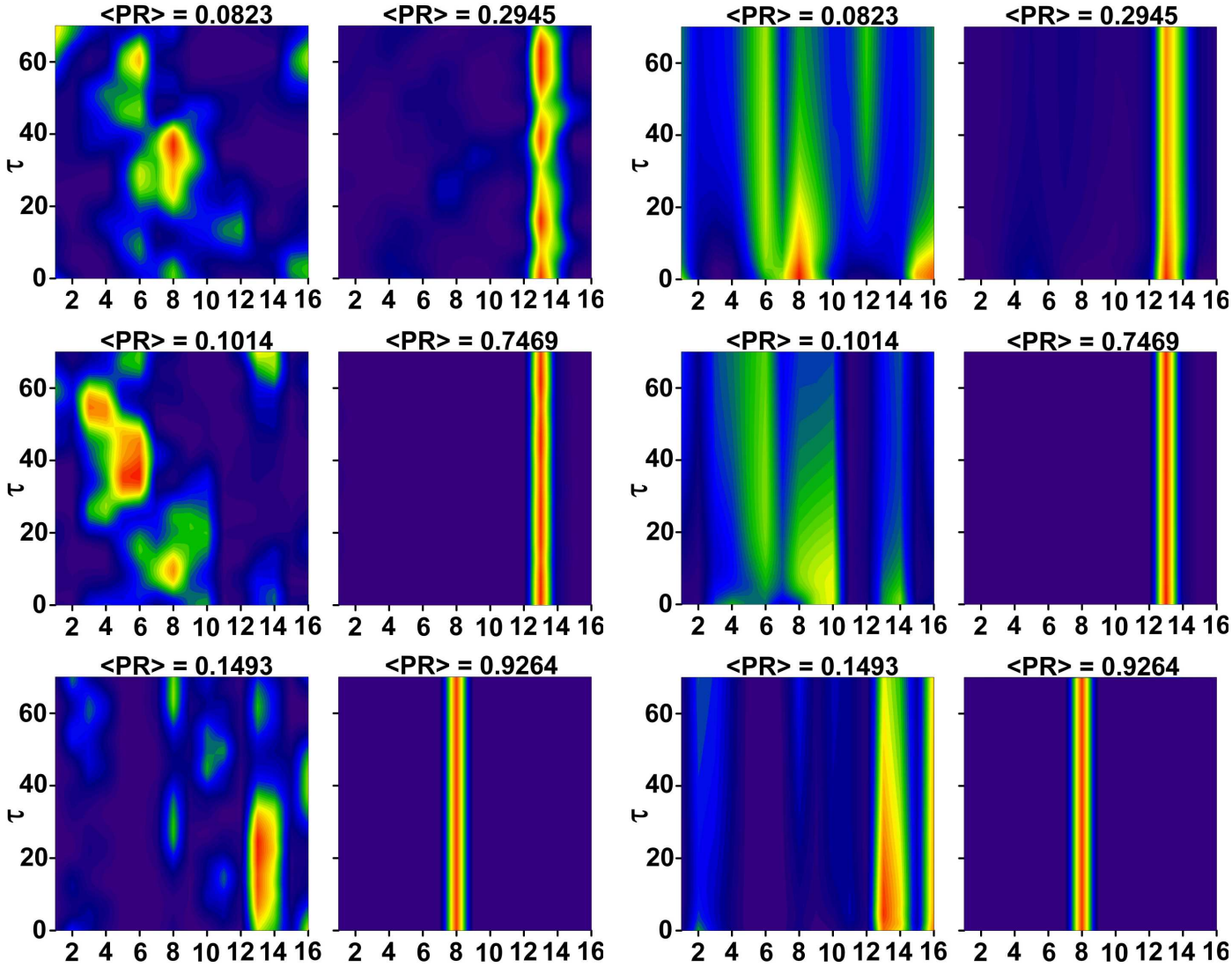

Fig. 6. The diagonal exciton density matrix elements of LH4 ring in the site representation ρ_{nn} without dynamic disorder (coherent dynamics) at low temperature $kT = 0.1\ J_0$ are shown as a function of time τ for the realizations of Gaussian uncorrelated static disorder in local excitation energies $\delta\varepsilon_n$ with lowest $\langle PR \rangle$ value (first column) and highest $\langle PR \rangle$ value (second column) – three different strengths of static disorder Δ = 0.1 J_0 (first row), 0.3 J_0 (second row), 0.6 J_0 (third row).

Fig. 7. The diagonal exciton density matrix elements of LH4 ring in the site representation ρ_{nn} with dynamic disorder effect taking into account at low temperature $kT = 0.1\ J_0$ are shown as a function of time τ for the realization of Gaussian uncorrelated static disorder in local excitation energies $\delta\varepsilon_n$ with lowest $\langle PR \rangle$ value (first column) and highest $\langle PR \rangle$ value (second column) – three different strengths of static disorder Δ = 0.1 J_0 (first row), 0.3 J_0 (second row), 0.6 J_0 (third row).

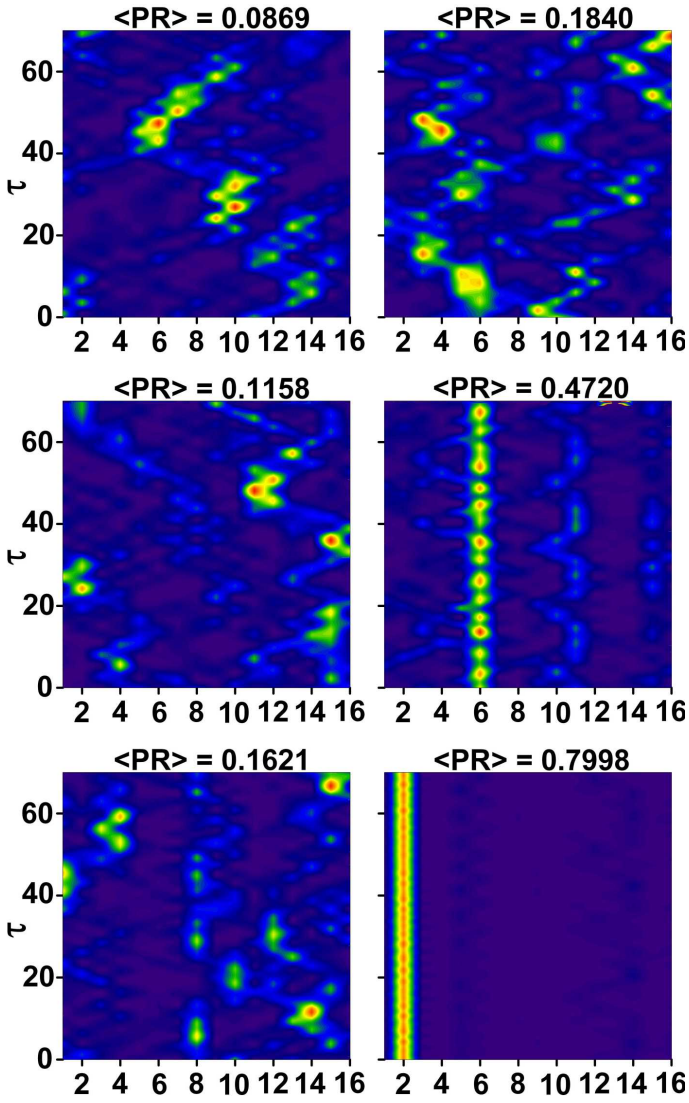

Fig. 8. The diagonal exciton density matrix elements of LH4 ring in the site representation ρ_{nn} without dynamic disorder (coherent dynamics) at room temperature $kT = 0.5\ J_0$ are shown as a function of time τ for the realizations of Gaussian uncorrelated static disorder in local excitation energies $\delta\varepsilon_n$ with lowest $\langle PR\rangle$ value (first column) and highest $\langle PR\rangle$ value (second column) – three different strengths of static disorder Δ = 0.1 J_0 (first row), 0.3 J_0 (second row), 0.6 J_0 (third row).

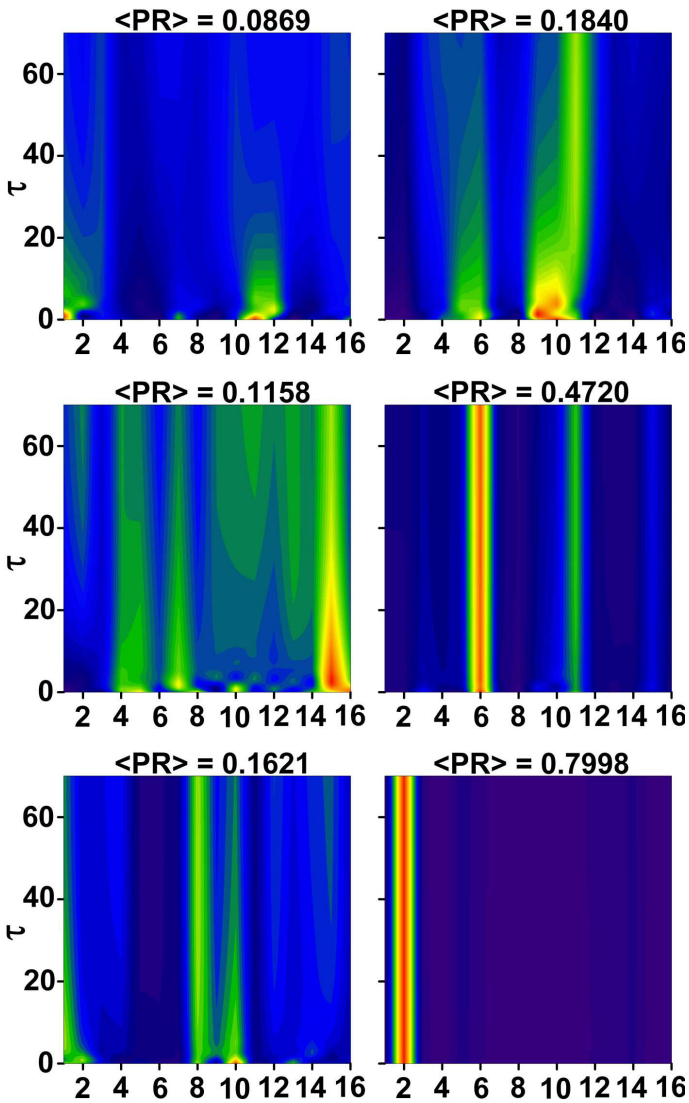

Fig. 9. The diagonal exciton density matrix elements of LH4 ring in the site representation ρ_{nn} with dynamic disorder effect taking into account at room temperature $kT = 0.5\ J_0$ are shown as a function of time τ for the realization of Gaussian uncorrelated static disorder in local excitation energies $\delta\varepsilon_n$ with lowest $\langle PR\rangle$ value (first column) and highest $\langle PR\rangle$ value (second column) – three different strengths of static disorder Δ = 0.1 J_0 (first row), 0.3 J_0 (second row), 0.6 J_0 (third row).

Fig. 4 shows the values of thermally averaged participation ratio $\langle PR\rangle$ for LH4 ring as a function of FL spectrum peak position at room temperature $kT = 0.5\ J_0$ and low one $kT = 0.1\ J_0$ calculated for 2000 realizations of the disorder. For comparison, the same as in Fig. 4 but for LH2 ring is presented in Fig. 5.

Dynamics of the diagonal exciton density matrix elements in site representation ρ_{nn} at room temperature $kT = 0.5\ J_0$ and low one $kT = 0.1\ J_0$ is shown in Fig. 6 – Fig. 9 for three above mentioned strengths of static disorder. Initial density matrix in eigenstate representation $\rho_{\alpha\beta}(t = 0)$ is chosen by us corresponding to coherent wavepacket with steady state (thermally equilibrated) populations P_α and arbitrary fixed phases φ_α [27],

$$\rho_{\alpha\beta} = \sqrt{P_\alpha P_\beta}\ \mathrm{e}^{\mathrm{i}(\varphi_\alpha - \varphi_\beta)}, \tag{20}$$

and

$$\rho_{\alpha\alpha} = P_\alpha \sim \mathrm{e}^{-\frac{\varepsilon_\alpha}{kT}}. \tag{21}$$

Timescale $\tau \in \langle 0; 70\rangle$ corresponds to $t \in (0; 1.4\ \mathrm{ps})$ or $(0; 1\ \mathrm{ps})$ for limit values of J_0 mentioned above. Contrary to [27] the dynamic disorder have been taken into account in our simulations. Fig. 6 and Fig. 8 show the coherent dynamics (without dynamic disorder) for the realizations of

static disorder with lowest and highest $\langle PR \rangle$ values. Fig. 7 and Fig. 9 show the same but with the dynamic disorder effect taking into account.

V. Conclusions

Software package *Mathematica* has been found by us very useful for the simulations of the molecular ring spectra. From the comparison of our simulated FL and OD spectra for LH4 ring (Fig. 1) with our previous results for LH2 ring [20] we can see that the spectral lines for LH4 ring are shifted to smaller wavelengths (higher energies).

The shift of fluorescence spectral line to higher wavelengths (lower energies) is visible for increasing strength of static disorder. It corresponds with the creation of the second peak in the fluorescence peak position distribution (Fig. 2).

Another difference can be found in widths of spectral line profiles. Absorption line of LH4 at low temperature $kT = 0.1\ J_0$ for small strength of static disorder is significantly wider then fluorescence one. On the other hand the absorption and fluorescence spectral lines have similar widths for LH2 ring [21].

If we compare the distributions of the participation ratios PR_α for LH4 ring (Fig 3) with the same for LH2 ring [23], we can conclude that localization of exciton eigenstates in LH4 ring is higher. Also correlation between PR_α value and single molecule FL spectrum peak position for LH4 ring is not evident in contrast with LH2 ring.

From Fig. 4 it can be seen growing of $\langle PR \rangle$ values in case of higher strength of static disorder for LH4 ring similarly as for LH2 (Fig. 5).

On the other hand, comparison of Fig. 4 and Fig. 5 shows significant differences in $\langle PR \rangle$ values for LH2 and LH4 rings. The participation ratio $\langle PR \rangle$ of LH4 ring for highest strength of static disorder ($\Delta = 0.6\ J_0$) reaches values about 0.9. Contrary $\langle PR \rangle$ of LH2 ring has only values about 0.5 for the same strength of static disorder. It also corresponds to more localized exciton states in LH4 ring.

From Fig. 6 – Fig. 9 we can see that different strengths of static disorder (different degree of localization $\langle PR \rangle$) produce different types of coherent excitation dynamics. The population distribution for small $\langle PR \rangle$ is more or less uniform, i.e., excitation can be found on any part of the ring. The wavepacket moves around the ring in this case. On the other hand, higher values of $\langle PR \rangle$ lead to higher localization of excitation on a smaller group of pigments or even on a single pigment. Excitation can be even totally localized on a single molecule without any migration to the other sites in case of highest $\langle PR \rangle$. If the dynamic disorder is taken into account, oscillations in exciton dynamics are suppressed. The dynamics can be characterized by relaxation. From comparison of Fig. 6, Fig. 7 with Fig. 8, Fig. 9, the slower exciton dynamics is visible in case of low temperature $kT = 0.1\ J_0$.

References

[1] G. McDermott et al., Crystal-structure of an integral membrane light-harvesting complex from photosynthetic bacteria, *Nature* 374, 1995, pp. 517–521.

[2] M. Z. Papiz et al., The structure and thermal motion of the B800-850 LH2 complex from Rps. acidophila at 2.0 Å over-circle resolution and 100 K: New structural features and functionally relevant motions, *J. Mol. Biol.* 326, 2003, pp. 1523–1538.

[3] W. P. M. de Ruijter, et al., Observation of the Energy-Level Structure of the Low-Light Adapted B800 LH4 Complex by Single-Molecule Spectroscopy, *Biophys. J.* 87, 2004, pp. 3413–3420.

[4] R. Kumble, R. Hochstrasser, Disorder-induced exciton scattering in the light-harvesting systems of purple bacteria: Influence on the anisotropy of emission and band → band transitions, *J. Chem. Phys.* 109, 1998, pp. 855–865.

[5] V. Nagarajan et al., Ultrafast exciton relaxation in the B850 antenna complex of Rhodobacter sphaeroides, *Proc. Natl. Acad. Sci. USA* 93, 1996, pp. 13774–13779.

[6] V. Nagarajan et al., Femtosecond pump-probe spectroscopy of the B850 antenna complex of Rhodobacter sphaeroides at room temperature, *J. Phys. Chem. B* 103, 1999, pp. 2297–2309.

[7] V. Nagarajan, W. W. Parson, Femtosecond fluorescence depletion anisotropy: Application to the B850 antenna complex of Rhodobacter sphaeroides, *J. Phys. Chem. B* 104, 2000, pp. 4010–4013.

[8] V. Čápek, I. Barvík, P. Heřman, Towards proper parametrization in the exciton transfer and relaxation problem: dimer, *Chem. Phys.* 270, 2001, pp. 141–156.

[9] P. Heřman, I. Barvík, Towards proper parametrization in the exciton transfer and relaxation problem. II. Trimer, *Chem. Phys.* 274, 2001, pp. 199–217.

[10] P. Heřman, I. Barvík, M. Urbanec, Energy relaxation and transfer in excitonic trimer, *J. Lumin.* 108, 2004, pp. 85-89.

[11] P. Heřman et al., Exciton scattering in light-harvesting systems of purple bacteria, *J. Lumin.* 94-95, 2001, pp. 447–450.

[12] P. Heřman, I. Barvík, Non-Markovian effects in the anisotropy of emission in the ring antenna subunits of purple bacteria photosynthetic systems, *Czech. J. Phys.* 53, 2003, pp. 579–605.

[13] P. Heřman et al., Influence of static and dynamic disorder on the anisotropy of emission in the ring antenna subunits of purple bacteria photosynthetic systems, *Chem. Phys.* 275, 2002, pp. 1–13.

[14] P. Heřman, I. Barvík, Temperature dependence of the anisotropy of fluorescence in ring molecular systems, *J. Lumin.* 122–123, 2007, pp. 558–561.

[15] P. Heřman, D. Zapletal, I. Barvík, Computer simulation of the anisotropy of fluorescence in ring molecular systems: Influence of disorder and ellipticity, in *Proc. IEEE 12th International Conference on Computational Science and Engineering (CSE '09)*, Vancouver, 2009, pp. 437–442.

[16] P. Heřman, I. Barvík, Coherence effects in ring molecular systems, *Phys. Stat. Sol. C* 3, 2006, 3408-3413.

[17] P. Heřman, D. Zapletal, I. Barvík, The anisotropy of fluorescence in ring units III: Tangential versus radial dipole arrangement, *J. Lumin.* 128, 2008, pp. 768-770.

[18] P. Heřman, I. Barvík, D. Zapletal, Computer simulation of the anisotropy of fluorescence in ring molecular systems: Tangential vs. radial dipole arrangement, *Lecture Notes in Computer Science* 5101, 2008, pp. 661-670.

[19] P. Heřman, D. Zapletal, I. Barvík, Lost of coherence due to disorder in molecular rings, *Phys. Stat. Sol. C* 6, 2009, 89-92.

[20] P. Heřman, D. Zapletal, J. Šlégr, Comparison of emission spectra of single LH2 complex for different types of disorder, *Physics Procedia* 13, 2011, pp. 14–17.

[21] P. Heřman, D. Zapletal, M. Horák, Computer simulation of steady state emission and absorption spectra for molecular ring, in *ADVCOMP2011, Proc.of the 5th International Conference on Advanced Engineering Computing and Applications in Sciences*, S. Omatu, S. G. Fabri, Eds., Lisbon: IARIA, 2011, pp. 1–6.

[22] D. Zapletal, P. Heřman, Computer simulation of fluorexcence spectra for molecular ring: exciton dynamics, in *Proceedings of the 13th WSEAS International Conference on Mathematical and Computational Methods in Science and Engineering (MACMESE '11)* WSEAS Press, 2011, pp. 182–187.

[23] D. Zapletal, P. Heřman, Simulation of molecular ring emission spectra: localization of exciton states and dynamics, *IJCMS* 6, 2012, pp. 144–152.

[24] M. Horák, P. Heřman, D. Zapletal, Computer simulation of spectra for molecular ring: LH4 - localization of exciton states, in *Advances in Mathematical and Computational Methods, Proceedings of the 14th WSEAS International Conference on Mathematical and Computational Methods in Science and Engineering (MACMESE '12)*, M. Iliescu, Ed., WSEAS Press, 2012, pp. 97–102.

[25] W. M. Zhang et al., Exciton-migration and three-pulse femtosecond optical spectroscopies of photosynthetic antenna complexes, *J. Chem. Phys.* 108, 1998, pp. 7763–7774.

[26] S. Mukamel, *Principles of nonlinear optical spectroscopy*. New York: Oxford University Press, 1995.

[27] V. I. Novoderezhkin, D. Rutkauskas, R. van Grondelle, Dynamics of the emission spectrum of a single LH2 complex: Interplay of slow and fast nuclear motions, *Biophys. J.* 90, 2006, pp. 2890–2902.

[28] A. G. Redfield, The Theory of Relaxation Processes, *Adv. Magn. Reson.* 1, 1965, pp. 1–32.

[29] D. Rutkauskas et al., Fluorescence spectroscopy of conformational changes of single LH2 complexes, *Biophys. J.* 88, 2005, pp. 422–435.

[30] D. Rutkauskas et al., Fluorescence spectral fluctuations of single LH2 complexes from *Rhodopseudomonas acidophila* strain 10050, *Biochemistry* 43, 2004, pp. 4431–4438.

[31] V. May, O. Kühn, *Charge and Energy Transfer in Molecular Systems*. Berlin: Wiley-WCH, 2000.

[32] O. Zerlauskiene et al., Static and Dynamic Protein Impact on Electronic Properties of Light-Harvesting Complex LH2, *J. Phys. Chem. B* 112, 2008, pp. 15883–15892.

[33] S. Wolfram, *The Mathematica Book*, 5th ed., Wolfram Media, 2003.

[34] A. A. Keller, Genetic Search Algorithms to Fuzzy Multiobjective Games: A Mathematica Implementation, in *10th WSEAS International Conference on Applied Computer Science*, Athens, 2010, pp. 351–359.

[35] D. Ustundag, M. Cevri, Bayesian Parameter Estimation of Sinusoids with Simulated Annealing, in *8th WSEAS International Conference on Signal Processing, Conputational Geometry and Artificial Vision*, Athens, 2008, pp. 106–112.

[36] M. C. Voicu, Computational Methods and Analytical Study for Detecting the Attractors of a Particular Type of k-Order, Nonlinear, Exchange Rate Models, in *13th WSEAS International Conference on Computers*, Athens, 2009, pp. 289–302.

[37] M. Trott, *The Mathematica GuideBook for Symbolics*. New York: Springer Science+Business Media, Inc., 2006.

[38] M. Trott, *The Mathematica GuideBook for Numerics*. New York: Springer Science+Business Media, Inc., 2006.

[39] P. Heřman, I. Barvík, D. Zapletal, Energetic disorder and exciton states of individual molecular rings, *J. Lumin.* 119-120, 2006, pp. 496–503.